Journal of the European Ceramic Society 38 (2018) 95–103

Contents lists available at ScienceDirect

Journal of the European Ceramic Society

journal homepage: www.elsevier.com/locate/jeurceramsoc

Full Length Article

Controlling microstructure and film growth of relaxor-ferroelectric thin films for high break-down strength and energy-storage performance

Minh D. Nguyen[a,b,*], Chi T.Q. Nguyen[b,c], Hung N. Vu[b], Guus Rijnders[a]

[a] MESA+ Institute for Nanotechnology, University of Twente, P.O. Box 217, 7500AE Enschede, The Netherlands
[b] International Training Institute for Materials Science (ITIMS), Hanoi University of Science and Technology, No. 1 Dai Co Viet Road, Hanoi 10000, Viet Nam
[c] Vietnam National University of Forestry, Chuong My District, Hanoi 10000, Viet Nam

ARTICLE INFO

Keywords:
Reloxor ferroelectrics
Thin films
Microstructure
Break-down strengths
Energy-storage performances

ABSTRACT

The relaxor ferroelectric $Pb_{0.9}La_{0.1}(Zr_{0.52}Ti_{0.48})O_3$ (PLZT) thin films were deposited using pulsed laser deposition, and their microstructures, break-down field strengths and energy storage performances were investigated as a function of the buffer layer and electrode. A large recoverable energy-storage density (U_{reco}) of 23.2 J/cm^3 and high energy-storage efficiency (η) of 91.6% obtained in the epitaxial PLZT film grown on $SrRuO_3/SrTiO_3$/Si are much higher than those in the textured PLZT film (U_{reco} = 21.9 J/cm^3, η = 87.8%) on $SrRuO_3/Ca_2Nb_3O_{10}$-nanosheet/Si and the polycrystalline PLZT film (U_{reco} = 17.6 J/cm^3, η = 82.6%) on Pt/Ti/SiO_2/Si, under the same condition of 1500 kV/cm and 1 kHz, due to the slim polarization loop and significant antiferroelectric-like behavior. Owing to the high break-down strength (BDS) of 2500 kV/cm, a giant U_{reco} value of 40.2 J/cm^3 was obtained for the epitaxial PLZT film, in which U_{reco} values of 28.4 J/cm^3 (at BDS of 2000 kV/cm) and 20.2 J/cm^3 (at BDS of 1700 kV/cm), respectively, were obtained in the textured and polycrystalline PLZT films. The excellent fatigue-free properties and high thermal stability were also observed in these films.

1. Introduction

Dielectric materials with high power density, fast charge/discharge, excellent charge/discharge efficiency and low cost have been extensively investigated for the potential application in advanced pulse power capacitors for electronics and electrical power systems, such as radar transmitters, laser, medical defibrillators and pacemakers [1–5]. Based on the physical principals, the materials with higher saturated polarization, smaller remanent polarization, and higher electrical break-down strength are the most promising candidates [6]. In general, the recoverable energy-storage density (U_{reco}) of a capacitor could be calculated from the polarization hysteresis (*P-E*) loops as the following equation:

$$U_{reco} = \int_{P_{r+}}^{P_{max}} E dP \tag{1}$$

where, E the applied electric field, P is polarization; P_{max} and P_{r+} are the maximum and positive remanent polarizations, respectively. Based on Eq. (1), it can be seen that not only large P_{max} and low P_{r+} (or low coercive field), but also high E, are desirable in order to get the high U_{reco} value for the practical applications. Due to the high break-down strength (BDS), the dielectric capacitors based on thin films have attracted increasing attention for high energy-storage performances.

Currently, the most studies on energy-storage performances are mainly focused on antiferroelectric films [1,2,7–9], due to the high maximum polarization and low remanent polarization. Ahn et al. [2] indicated that the larger U_{reco} (32.7 J/cm^3) and high η (~90%) values can be obtained in the $Pb_{0.97}Y_{0.02}[(Zr_{0.6}Sn_{0.4})_{0.925}Ti_{0.075}]O_3$ (PYZST) antiferroelectric thin films, under an applied electric field of 1800 kV/cm. Recently relaxor ferroelectric films have been also considered as a potential candidate for use in pulse power applications [4,5,10–14]. Hao et al. [13] reported a high energy storage density of about 11.5 J/cm^3 and an energy efficiency of about 52.5% in relaxor-ferroelectric $Pb_{0.91}La_{0.09}(Ti_{0.65}Zr_{0.35})O_3$ thin films on Pt/Ti/SiO_2/Si (Pt/Si), under an electric field of 1000 kV/cm; Tong et al. [14] studied relaxor-ferroelectric $Pb_{0.92}La_{0.08}(Ti_{0.52}Zr_{0.48})O_3$ films and achieved U_{reco} and η values of about 12.0 J/cm^3 and 70.0% for the films on LNO/Ni (at 1000 kV/cm). Wang et al. [10] showed a high U_{reco} of 31 J/cm^3 and η of 64% in the $0.8Pb(Mg_{1/3}Nb_{2/3})O_3$-$0.2PbTiO_3$ relaxor ferroelectric thin films under an electric field of 2000 kV/cm. Moreover, the energy-storage performance was also enhanced by the doping of Mn in the $0.7(Nb_{0.5}Bi_{0.5})TiO_3$-$0.3SrTiO_3$ relaxor ferroelectric thin films, in which the high U_{reco} of 27 J/cm^3 and η of 44% were obtained under an applied electric field of 1894 kV/cm for 1% Mn doping [4].

* Corresponding author at: MESA+ Institute for Nanotechnology, University of Twente, P.O. Box 217, 7500AE Enschede, The Netherlands.
E-mail address: d.m.nguyen@utwente.nl (M.D. Nguyen).

http://dx.doi.org/10.1016/j.jeurceramsoc.2017.08.027
Received 17 July 2017; Received in revised form 14 August 2017; Accepted 18 August 2017
Available online 24 August 2017
0955-2219/ © 2017 Elsevier Ltd. All rights reserved.

Although the recoverable energy storage densities in relaxor ferroelectric films are comparable to those of antiferroelectric films, the above mentioned energy efficiencies are still significantly lower. In recent studies, we indicated that the high U_{reco} and η values can be obtained in the epitaxial relaxor ferroelectric $Pb_{0.9}La_{0.1}(Zr_{0.52}Ti_{0.48})O_3$ (PLZT) thin films, with coexistence of ferroelectric (FE) and antiferroelectric-like (AFE) behaviors, grown on $SrRuO_3/SrTiO_3$/Si (STO/Si) and $SrRuO_3/SrTiO_3$ (STO) substrates using pulsed laser deposition [15,16]. The U_{reco} and η values of these above thin films were 13.7 J/cm^3 and 88.2%, 12.7 J/cm^3 and 88.4%, respectively, while the PYZST thin films had U_{reco} of 14.6 J/cm^3 and η = 91.3% [2], under the same applied electric field of 1000 kV/cm. Even the energy-storage performances of relaxor ferroelectric PLZT thin films on STO and STO/Si substrates were similar to those in the antiferroelectric PYZST thin films, however, STO substrate is impractical for use in actual devices due to their high cost and lack of large substrate sizes, and where the $SrTiO_3$ buffer-layer process on silicon, generally performed by Molecular Beam Epitaxy, is very delicate and slow. In order to investigate the growth of PLZT thin films on Si substrates for industrial applications, we have studied the energy-storage performances of PLZT thin films on $Ca_2Nb_3O_{10}$ nanosheet buffered Si (CNO/Si) and $Pt/Ti/SiO_2$/Si (Pt/Si) substrates. In the previous studied, we indicated that the properties of $Pb(Zr_{0.52}Ti_{0.48})O_3$ (PZT) thin-film devices can be enhanced by using a monolayer of CNO nanosheet deposited on Si substrates using Langmuir-Blodgett (LB) method and are well comparable with devices using more conventional oxide buffer layers (stacks), such as YSZ, CeO_2/YSZ or $SrTiO_3$ on Si [17]. Moreover, the CNO nanosheets can be deposited on the Si wafer-scales (such as 4-inch), therefore the CNO/Si and also Pt/Si have found widespread use in the production of microsystems with PZT or PLZT thin films.

The microstructures, ferroelectrics, break-down strengths and energy-storage performances of $Pb_{0.9}La_{0.1}(Zr_{0.52}Ti_{0.48})O_3$ (PLZT) thin films grown on CNO/Si and Pt/Si have been investigated and compared with the thin film on STO/Si in this present work. Moreover, reliability of the stored information in PLZT thin films as a function of working cycles and thermal stability will be also mentioned. It is found that, although the energy-storage performance of the PLZT thin film grown on STO/Si is still superior, the PLZT thin film deposited on CNO/Si posses energy-storage performance of comparable value. These findings could be important for further integration of PLZT capacitors on Si wafer-scale with low cost for industrial applications.

2. Experimental procedure

Relaxor ferroelectric $Pb_{0.9}La_{0.1}(Zr_{0.52}Ti_{0.48})O_3$ (PLZT) thin films were deposited on $SrRuO_3/SrTiO_3$/Si (STO/Si), $SrRuO_3/Ca_2Nb_3O_{10}$/Si (CNO/Si) and $Pt/Ti/SiO_2$/Si (Pt/Si) substrates using a pulsed laser deposition (PLD) method. The 8-nm-thick epitaxial $SrTiO_3$ (STO) buffer layer was grown by reactive molecular-beam epitaxy on Si substrates and acts as a seed layer for highly (001)-oriented epitaxial growth of the subsequent perovskite layers [18]. The $Ca_2Nb_3O_{10}$ (CNO) nanosheets were fabricated on Si substrates by exfoliation of layered protonated calcium niobate ($HCa_2Nb_3O_{10}{\cdot}1.5H_2O$) by the Langmuir-Blodgett deposition method [19,20]. In order to prepare the Pt/Si substrates, a 125-nm-thick Pt bottom electrodes and 15-nm-thick Ti adhesive layers were deposited at room temperature by DC magnetron sputtering on a 500-nm-thick SiO_2 layer formed through wet-oxidation at 1100 °C. To prevent the formation of pyrochlore phases, a thin nucleation layer of $LaNiO_3$ (LNO, 10 nm, using PLD) was inserted between the Pt bottom electrode and the PLZT film [21].

The optimized deposition conditions of the PLZT thin films were: laser repetition rate 10 Hz, energy density 2.5 J/cm^2, oxygen pressure 0.1 mbar and substrate temperature 600 °C [22]. For the top and bottom $SrRuO_3$ (SRO) electrodes the conditions were: laser repetition rate 4 Hz, energy density 2.5 J/cm^2, oxygen pressure 0.13 mbar and substrate temperature 600 °C. The thickness of top and bottom SRO electrodes is about 100 nm.

Crystallographic properties of the thin films were analyzed by x-ray θ-2θ scans (XRD) and omega scans using a PANalytical X-ray diffractometer with Cu-$K\alpha$ radiation (wavelength: 1.5405 Å) operating at 45 kV and 40 mA. Atomic force microscopy (AFM: Bruker Dimension Icon) and cross-sectional high-resolution scanning electron microscopy (HRSEM: Zeiss-1550) were performed to investigate the morphology, microstructure and thickness of the as grown thin films. For electrical measurements, 100 × 100 μm^2 capacitors were patterned with a standard photolithography process and structured by argon-beam etching of the top-electrodes and wet-etching (*HF-HCl* solution) of the PLZT thin films. The polarization hysteresis loop measurements were performed with the ferroelectric mode of the aixACCT TF-2000 Analyzer at 1 kHz and various amplitudes. A Süss MicroTech PM300 manual probe station equipped with a Keithley 4200 Semiconductor Characterization System was used for the capacitance measurement. The capacitance-electric field (*C-E*) curves were measured up to a *dc*-electric field of ± 200 kV/cm and with a 1 kHz frequency *ac*-electric field of 2 kV/cm amplitude. The corresponding dielectric constants were calculated from the *C-E* curves. All measurements were performed at room temperature.

3. Results and discussion

Fig. 1 shows the XRD patterns of PLZT thin films on STO/Si, CNO/Si and Pt/Si substrates. It indicates that the thin film on STO/Si exhibits (001) orientation. Moreover, the epitaxial growth of PLZT thin film on STO/Si substrate can be observed from the phi-scan measurement, in which a 45° shift of the PLZT[101] reflections with respect to the Si [202] reflections with a fourfold rotational symmetry is found, indicating that the PLZT unit cells are rotated in-plane over 45° with respect to the Si lattice (Fig. 2(b)). The full-widths at half maximum ($FWHM_\omega$) of the rocking curve of the PLZT(002) peak in Fig. 2(a) was 0.42°, indicating a good crystalline quality of the film. The width of the rocking curves is a measure of the range over which the lattice structure in the different grains tilts with respect to the film normal [23] and is therefore an indication of the homogeneity of the films.

Even the PLZT thin film is not epitaxially grown on CNO/Si, but it has a highly textured (001) orientation with a minor (110) peak. The FWHM value of PLZT(002) peak is about 0.46° and it is indicated that the alignment of the PLZT crystal planes was found to be slightly better in the epitaxial film grown on STO/Si. Whereas, the polycrystalline growth with the mixed orientation is observed in the PLZT thin film grown on Pt/Si (Fig. 1(c)).

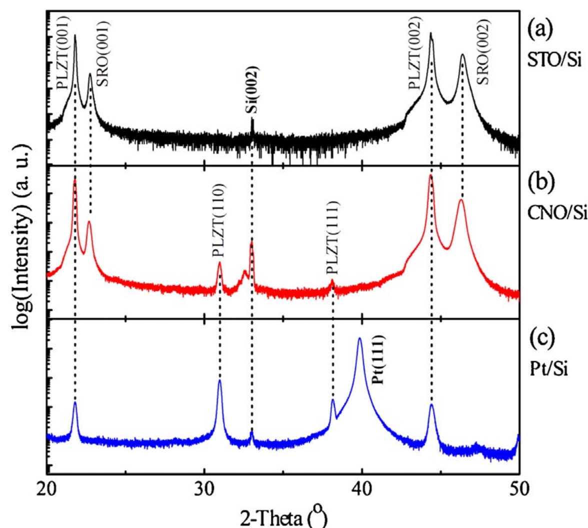

Fig. 1. XRD patterns of PLZT thin films grown on (a) STO/Si, (b) CNO/Si and (c) Pt/Si substrates.

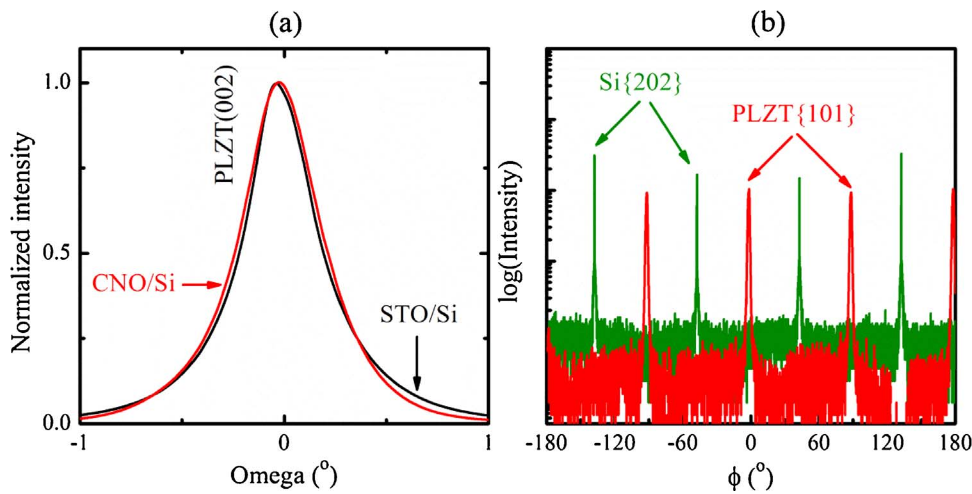

Fig. 2. (a) Rocking curves of (002) peaks of PLZT thin films grown on STO/Si and CNO/Si. (b) Phi-scan of PLZT thin film grown on STO/Si.

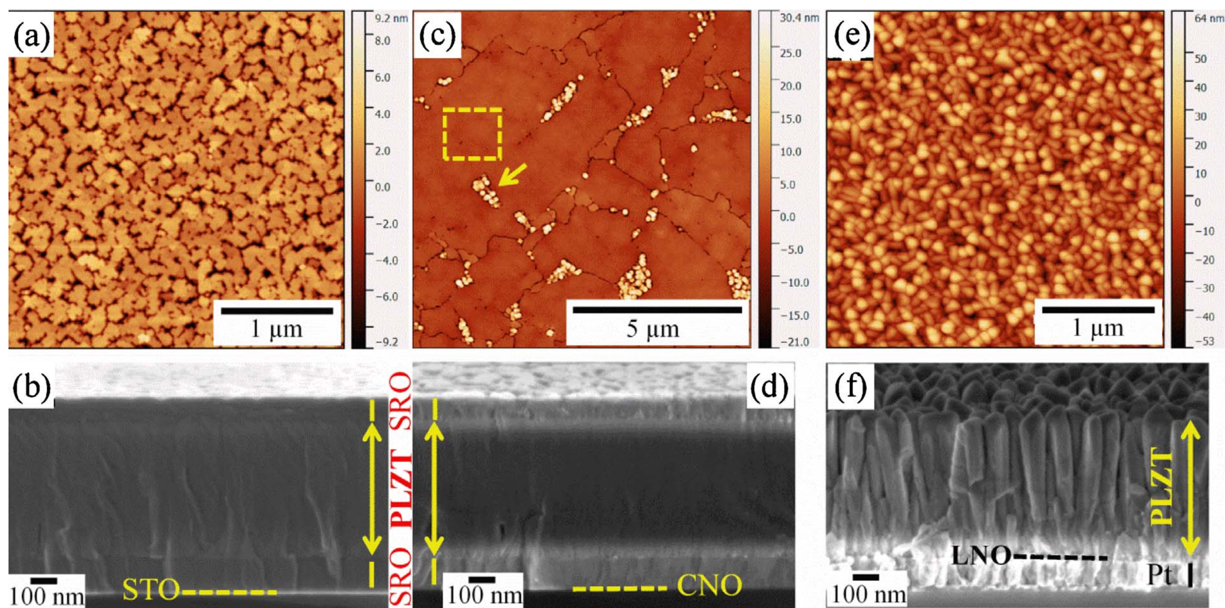

Fig. 3. AFM and cross-sectional SEM images of PLZT thin films grown on (a,b) STO/Si, (c,d) CNO/Si and (e,f) Pt/Si substrates. The dashed-box and arrow in (c) indicate the film with dense and columnar structures, respectively, on the CNO nanosheet and the gap between the nanosheets.

The microstructure and surface morphology of PLZT thin films are investigated using cross-sectional SEM and AFM, as shown in Fig. 3. Fig. 3(b) and (d) shows a very dense microstructure in the epitaxial and textured thin films, however, the polycrystalline columnar structure with a predominantly (110)-orientation is formed along lines arises from the edges of the nanosheets in the textured film (Fig. 3(c)-(d)). This structure was ascribed to a different nucleation density and growth at the edges of the nanosheets and the in-plane orientation mismatch of the single crystals grown on top of neighbouring nanosheets [17]. Fig. 3(f) reveals the columnar growth in the thin film grown on Pt/Si. Root-mean-square (R_{rms}) roughness values were calculated from the AFM measurements and are about 2.6, 3.9 (0.9 nm for the film deposited on top of nanosheet, as shown in the dashed-box in Fig. 3(c)) and 14.7 nm for the thin films grown on STO/Si, CNO/Si and Pt/Si, respectively. The cross-sectional SEM images also indicate that the thickness of PLZT thin films grown on STO/Si, CNO/Si and Pt/Si, respectively, are about 500, 506 and 518 nm.

The room-temperature leakage current densities for PLZT thin films are plotted against the applied electric field and shown in Fig. 4(a). Compared with the polycrystalline PLZT thin film on Pt/Si, the higher values of the leakage current are realized in textured and epitaxial PLZT thin films grown on CNO/Si and STO/Si. The change in the leakage current can be explained by the difference in the microstructure from the compact and dense structure in the epitaxial and textured thin films to the grain-columnar structure in the polycrystalline thin film. At $E = 100$ kV/cm, the leakage current densities are 6.4×10^{-6} A/cm^2, 1.1×10^{-6} A/cm^2, and 1.1×10^{-7} A/cm^2 for the epitaxial, textured and polycrystalline thin films, respectively. A good epitaxial thin film is associated to a low resistivity due to the larger concentration of free carriers (with low resistivity) and thus the current density is high. In polycrystalline thin film, larger amount of structural defects, especially the grain boundaries, affect the charge transport as the trapping carriers (low concentration) and/or scattering the carriers (low mobility) [24]. This leads to an enhancement of the resistivity and as a result the lower current density is obtained in the polycrystalline thin film. Meanwhile, the current density in the textured thin film is lower than that in the epitaxial thin film (but higher than the polycrystalline thin film), due to the presence of the columnar growth areas happen on parts of the Si substrate that are not covered by nanosheets (Table 1).

In order to understand the change in leakage current in PLZT thin films, the conduction mechanism is investigated. Fig. 4(b) indicates the dependence of leakage current density (J) as a function of electric field

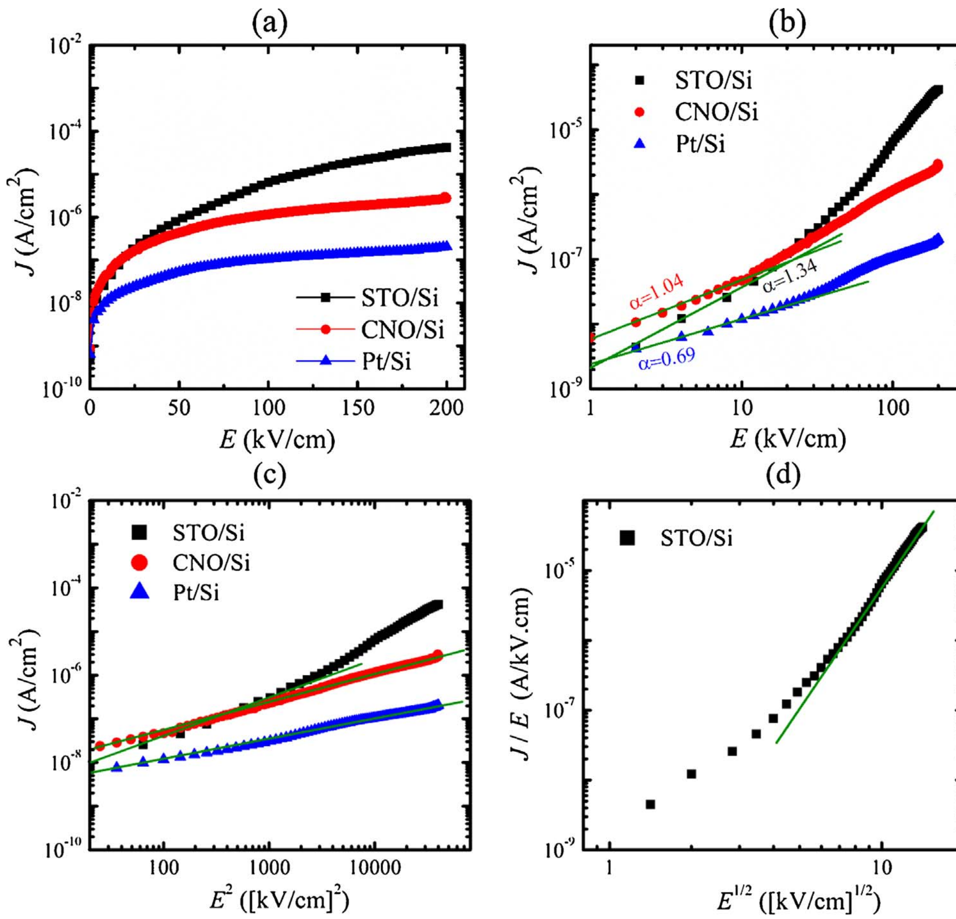

Fig. 4. (a) Leakage current density − electric field (*J-E*), (b) logarithmic plots of the dependence of *J* as a function of *E*, and (c) *J-E* characteristics in the form of the space charge limited current (SCLC), of PLZT thin films on SRO/STO/Si, SRO/CNO/Si and Pt/Si substrates. (d) Poole-Frenkel (PF) emission of PLZT thin film on STO/Si substrate.

(E) in logarithmic scale for PLZT thin films. It is indicated that the similar variation of log(J) with log(E) is observed in the textured and polycrystalline PLZT thin films. It consists of a low field linear region and a high field nonlinear region. In the low field region ($E < 20$ kV/cm) in Fig. 4(b), the thin films show Ohmic's contact. At room temperature, it can be assumed that enough charge carriers are present within the films, so as to contribute to the conduction process and hence a linear field dependence of conductivity can be observed. Above 20 kV/cm, the currents increase non-linearly which implies that the current conduction is governed by the other mechanisms. Fig. 4(c) indicates that the leakage current in the textured and polycrystalline thin films is dominated by space charge limited current (SCLC) mechanism. Under SCLC, the carriers form a freely moving space charge due to the reduced conductivity of the insulating or ferroelectric layer and the number of the free carriers causes an electric field gradient, which limits the current density. The SCLC current is related to E by the following relation [25]:

$$J_{SCLC} = \frac{9}{8}\mu\varepsilon_0\varepsilon_r\frac{E^2}{d^3} \quad (2)$$

where, μ is the mobility of the charge carriers and d is the film thickness. ε_0 ($=8.854 \times 10^{-12}$ F/m) and ε_r are the vacuum permittivity and

Table 1
Recoverable energy storage density (U_{reco}) and energy storage efficiency (η) of the antiferroelectric and relaxor ferroelectric thin films.

Films[a]	Substrates	Fabrication technique	Electric field (kV/cm)	U_{reco} (J/cm^3)	η (%)	Refs.
(AFE) $Pb_{0.97}Y_{0.02}[(Zr_{0.6}Sn_{0.6})_{0.925}Ti_{0.075}]O_3$	Pt/Si	PLD	1000	14.6	91.3	[2]
			1800[b]	32.7	90	
(AFE) $Pb_{0.97}La_{0.02}(Zr_{0.95}Ti_{0.05})O_3$	Pt/Si	Sol-gel	1850[b]	26.8	62.5	[7]
(RFE) $0.8Pb(Mg_{1/3}Nb_{2/3})O_3$-$0.2PbTiO_3$	Pt/Si	Sputtering	1000	13.6	65	[10]
			2000[b]	31	64	
(RFE) $(Pb_{0.91}La_{0.09})(Zr_{0.65}Ti_{0.35})O_3$	$LaNiO_3$/Si	Sol-gel	1000	10	64	[11]
			1185[b]	11.9	63.8	
(RFE) $(Pb_{0.91}La_{0.09})(Zr_{0.65}Ti_{0.35})O_3$ doped with 1% Mn	$LaNiO_3$/Si	Sol-gel	1000	15	68	[11]
			1679[b]	30.8	70	
(RFE) $Pb_{0.9}La_{0.1}(Zr_{0.52}Ti_{0.48})O_3$	Pt/Si	PLD	1000	11.7	82.3	This study
			1700[b]	20.2	79.6	
(RFE) $Pb_{0.9}La_{0.1}(Zr_{0.52}Ti_{0.48})O_3$	SRO/CNO/Si	PLD	1000	13.5	87.7	This study
			2000[b]	28.4	85.8	
(RFE) $Pb_{0.9}La_{0.1}(Zr_{0.52}Ti_{0.48})O_3$	SRO/STO/Si	PLD	1000	14.2	92.2	This study
			2500[b]	40.2	83.8	

[a] AFE – Antiferroelectric; RFE – Relaxor ferroelectric.
[b] Break-down strength (BDS) value.

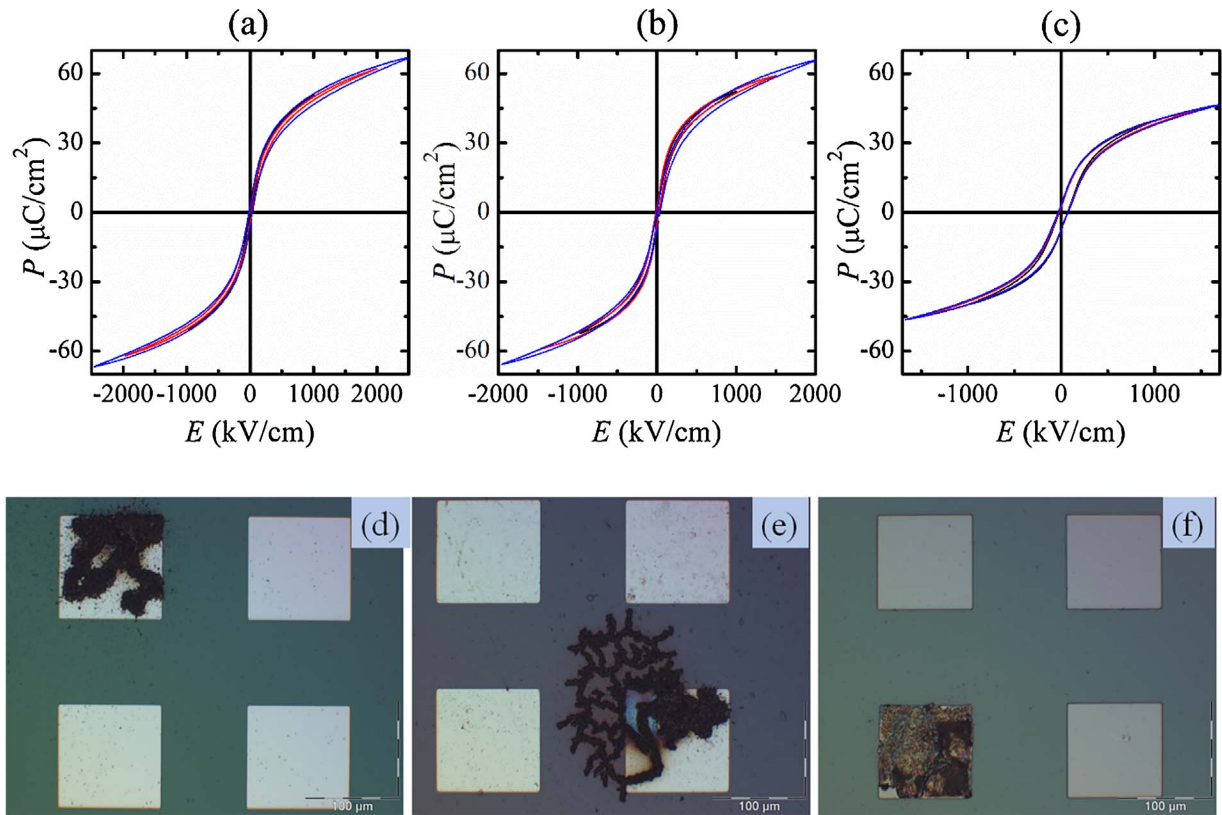

Fig. 5. *P–E* hysteresis loops of PLZT thin films grown on (a) STO/Si, (b) CNO/Si and (c) Pt/Si substrates, measured to their critical break-down strength (BDS). Optical images of broken capacitors: (d) epitaxial thin film on STO/Si at electric field of 2600 kV/cm, (e) textured thin film on CNO/Si at 2100 kV/cm and (f) polycrystalline thin film on Pt/Si at 1800 kV/cm.

the dielectric constant of the ferroelectric layer, respectively.

Similar to the textured and polycrystalline thin films, the current in the epitaxial thin film is also determined by the Ohmic's contact at low electric field ($E < 15$ kV/cm). However, the non-linearity at a high electric field region is combined effect of the SCLC mechanism (15 kV/cm < E < 50 kV/cm, Fig. 4(c)) and the Poole-Frenkel (PF) emission at $E > 50$ kV/cm (Fig. 4(d)). In the case of the PF emission, the electronic conduction as a bulk-controlled conduction mechanism through an insulator can occur due to the hopping of the charge carriers from one trap to another under a bias field. The PF current is given by the equation [26]:

$$J_{PF} = BE\exp\left(-\frac{q\varphi_t}{k_B T}\right)\exp\left[\left(\frac{q^3}{4\pi\varepsilon_0\varepsilon_r}\right)^{1/2}\frac{\sqrt{E}}{k_B T}\right] \tag{3}$$

where, B is a constant and ϕ_t is the trap level. T is the measuring temperature, k_B is the Boltzmann's constant, q and ϕ_B are the electronic charge and the Schottky barrier height, respectively.

The ferroelectric polarization intensity is also a key factor affecting the energy storage property. Fig. 5(a)–(c) shows the polarization (*P-E*) hysteresis loops of PLZT thin films on STO/Si (epitaxial film), CNO/Si (textured film) and Pt/Si (polycrystalline film) substrates measured to their critical break-down strength (BDS). It is noted that the slip *P-E* loops are observed in the epitaxial and textured thin films while the polycrystalline thin film has a slightly opened *P-E* loop. In order to define the BDS values in the thin-film capacitors, the *P-E* loops will be measured from the low applied electric field (such as 200 kV/cm) to the electric field where the thin-film capacitors are broken with an increased step of 100 kV/cm. The BDS value is the maximum applied electric field where the thin-film capacitor is still active. In this study, The BDS values are about 2500, 2000 and 1700 kV/cm, respectively, for the epitaxial, textured and polycrystalline PLZT thin films. Beyond on these values, the higher fields of 2600, 2100 and 1800 kV/cm for these above thin films, respectively, led to break-down of the thin films, as shown in Fig. 5(d)–(f).

The relationship between the break-down strength and leakage current in the ferroelectric films has been investigated. In general, the larger electric field can be applied to the films which have lower leakage current when the same electrodes are used. In this study, however, the polycrystalline PLZT thin film has a lower BDS value even the leakage current is much smaller than that in the epitaxial and textured thin films. The lower BDS value in the polycrystalline thin film in this case can be explained by the different electrodes, in which the Pt is used in the polycrystalline thin film and conductive SRO is used in the epitaxial and textured thin films. Pt is known as a catalyst for the hydrogen production through water vapor in the environmental humidity [27]. The penetration of hydrogen can induce structural degradation in various ways as described in the previous studies [28,29]. In this case, the hydrogen induced the break-down strength degradation in the polycrystalline thin film seems mainly to happen at the columnar grain boundaries.

In order to compare the ferroelectric properties and energy storage performances of PLZT thin films with different microstructures, the polarization hysteresis (*P-E*) measurements were performed at the same applied electric field of ± 1500 kV/cm and 1 kHz frequency, as shown in Fig. 6(a). The energy-stored per unit volume ($U_{store} = \int_{P_{r-}}^{P_{max}} EdP$), recoverable energy-storage density ($U_{reco} = \int_{P_{r+}}^{P_{max}} EdP$) and energy-storage efficiency ($\eta(\%) = 100 \times U_{reco}/U_{store}$) are calculated from the *P-E* loops (Fig. 6(a)) and shown in Fig. 6(b). It can be clearly found that the U_{store} values are similar for the epitaxial and textured thin films, but the U_{reco} value in the epitaxial thin film is higher due to the slimmer *P-E* loop, and resulting in a higher energy-storage efficiency (η). The U_{reco} and η values are 23.2 J/cm^3 and 91.6%, and 21.9 J/cm^3 and 87.8%,

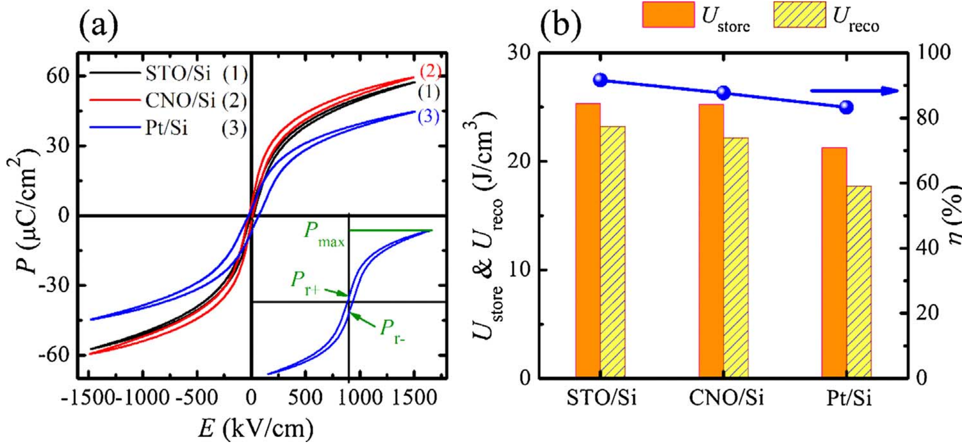

Fig. 6. (a) *P–E* hysteresis loops and (b) energy-stored per unit volume (U_{store}), recoverable energy-storage density (U_{reco}) and energy-storage efficiency (η), of the PLZT thin films grown on STO/Si, CNO/Si and Pt/Si substrates. The measurements were performed at ± 1500 kV/cm and 1 kHz frequency.

respectively, for the epitaxial and textured thin films. For polycrystalline thin film, the more opened *P-E* loop with low maximum polarization leads to the low energy-storage performances (U_{store} = 21.3 J/cm^3, U_{reco} = 17.6 J/cm^3 and η = 82.6%) under the same measured conditions.

From the above *P-E* ferroelectric hysteresis loops of PLZT thin films, evidently slim loops, which are typical of relaxor ferroelectric materials [30], are observed. Moreover, all the thin films exhibit double loops, demonstrating their antiferroelectric (AFE)-like behaviors. In order to verify the significance of AFE-like behavior in the relaxor PLZT thin films, the electric field dependence of switching current and capacitance curves were investigated (see Fig. 7). It is indicated that the double-butterfly-shaped *C-E* curves with a valley and four switching peaks in the switching current measurements were detected. On the other hand, the AFE-like behaviors are observed in these relaxor films. The AFE-like behavior in the epitaxial thin film is more dominant than that in the textured and polycrystalline thin films due to the sharper peak in the switching current, as shown in Fig. 7(a).

Fig. 8 illustrates the field-dependent energy-storage performance of the PLZT thin films. As desired, the U_{store} and U_{reco} values of all the thin films increase almost linearly with the electric field. As the applied field increased from 200 to 1500 kV/cm, the U_{store} values in the epitaxial and textured thin films are similar but the U_{reco} values in the textured thin film are slightly smaller, and the η values in the textured thin films are then lower than those in the epitaxial thin films at the same applied field. The energy-storage efficiency is relative stable in the textured thin film ($\eta \approx$ 85.4–87.8%) in the range from low field to its BDS (2000 kV/cm) and from low field to 2000 kV/cm for the epitaxial thin film ($\eta \approx$ 91.0–92.6%). Meanwhile, the energy-storage efficiency of the polycrystalline thin film is slightly decreased with increasing applied field, from 84% at low electric field (200 kV/cm) to 80% at its BDS value (1700 kV/cm). As can be seen, the epitaxial thin film has a large

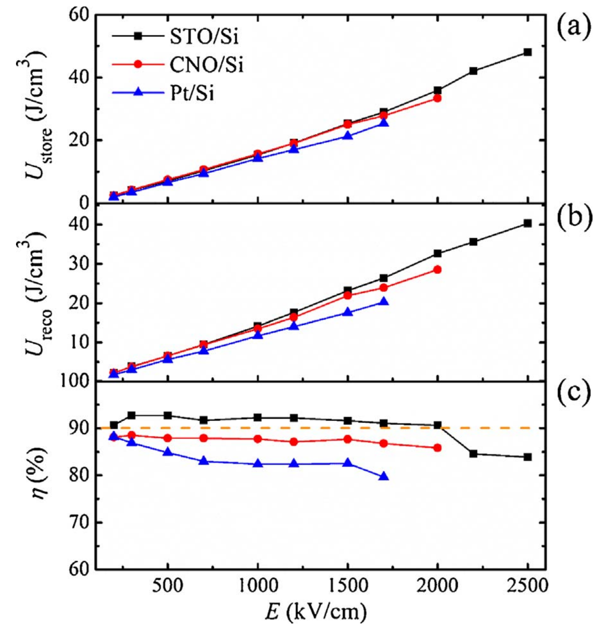

Fig. 8. Electric field dependence of (a) energy-stored per unit volume (U_{store}), (b) recoverable energy-storage density (U_{reco}) and (c) energy-storage efficiency (η), calculated from the above *P-E* loops of the PLZT thin films on STO/Si, CNO/Si and Pt/Si substrates.

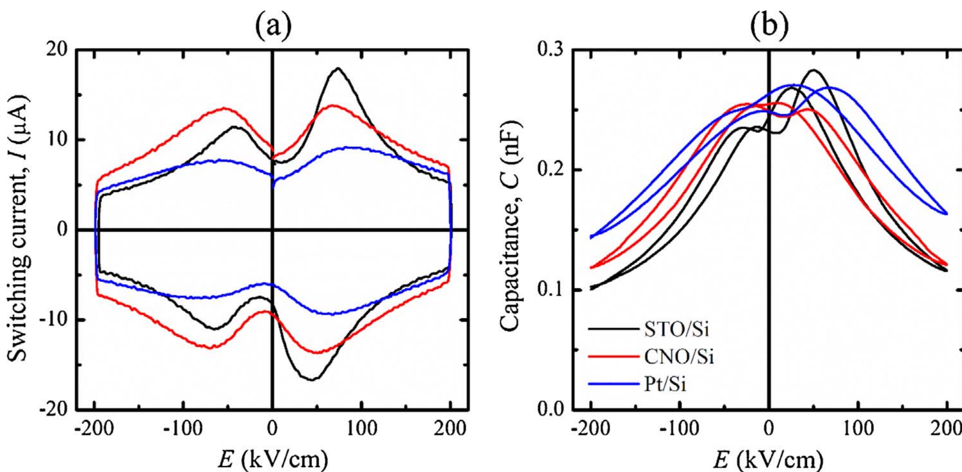

Fig. 7. (a) Switching current – electric field and (b) capacitance – electric field (*C-E*) curves, of PLZT thin films on STO/Si, CNO/Si and Pt/Si substrates. The measurements were performed at ± 200 kV/cm and 1 kHz frequency.

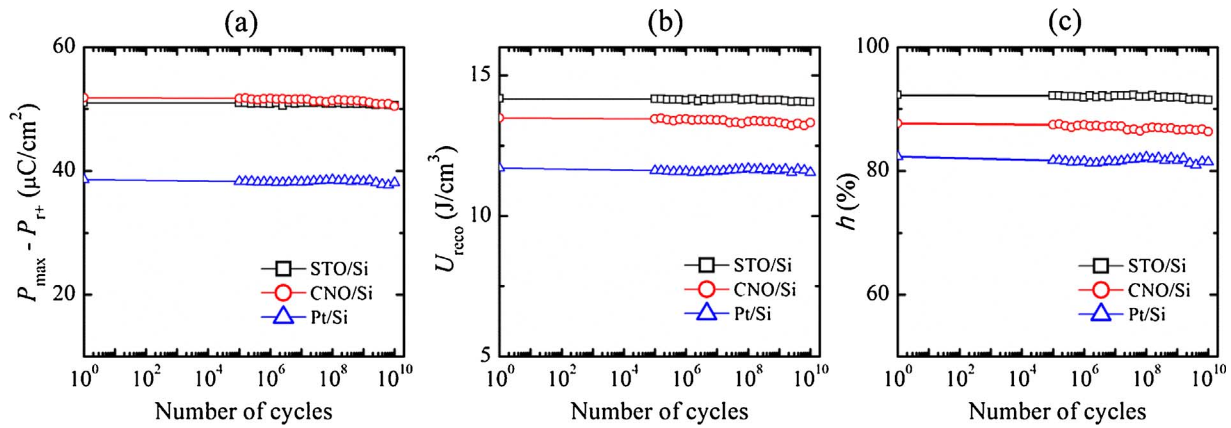

Fig. 9. Working cycles dependence of (a) net polarization ($P_{max} - P_{r+}$), (b) recoverable energy-storage density (U_{reco}) and (c) energy-storage efficiency (η), calculated from the *P-E* loops measured at an applied electric field of 1000 kV/cm and 1 kHz. The fatigue testing was performed by applying a bipolar electric field of 100 kV/cm and at 100 kHz.

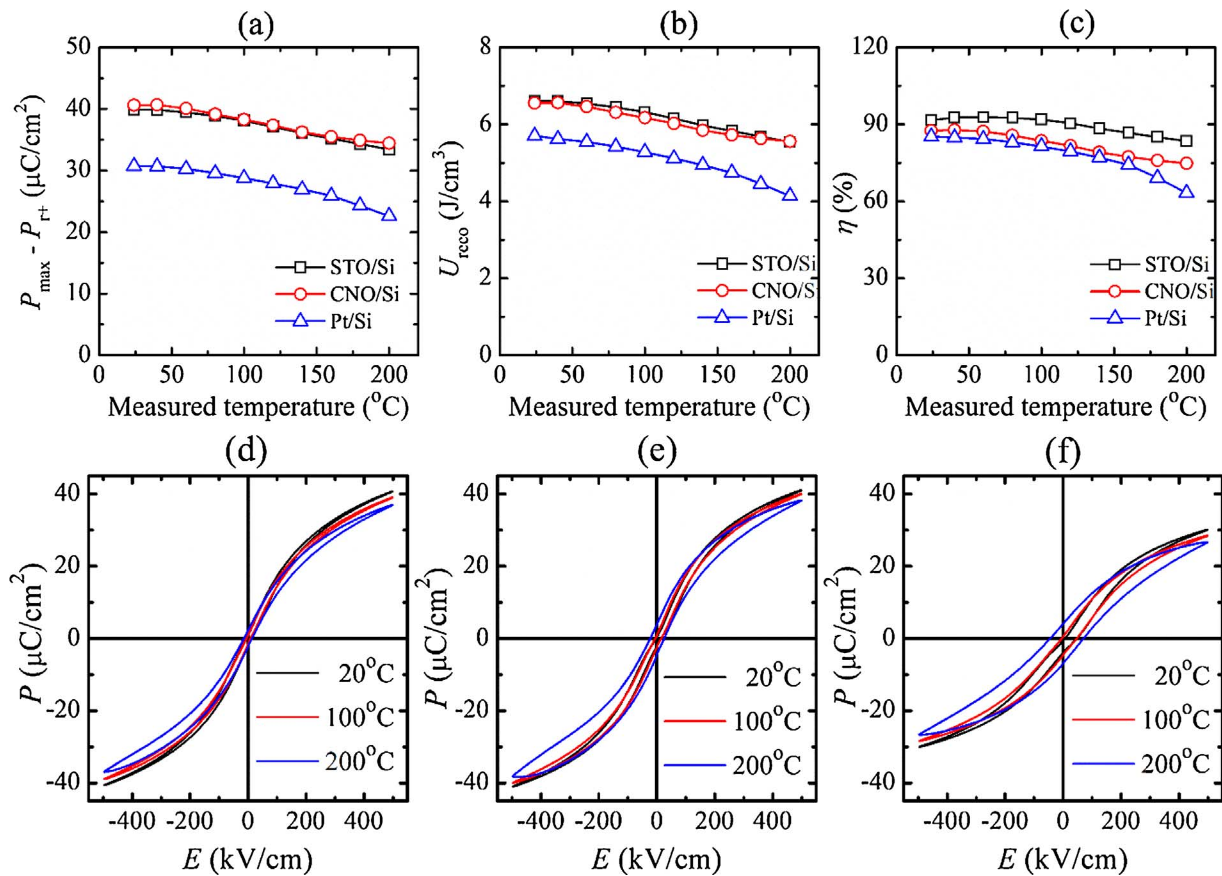

Fig. 10. Temperature dependence of (a) net polarization ($P_{max} - P_{r+}$), (b) recoverable energy-storage density (U_{reco}) and (c) energy-storage efficiency (η), calculated from the *P-E* loops of (d) epitaxial, (e) textured and (f) polycrystalline thin films, measured at 500 kV/cm and 1 kHz.

U_{reco} of 32.6 J/cm^3 with a high η of 90.6% under an applied field of 2000 kV/cm. Both U_{reco} and η values obtained in the epitaxial thin films in this study are similar to those in the $Pb_{0.97}Y_{0.02}[(Zr_{0.6}Sn_{0.4})_{0.925}Ti_{0.075}]O_3$ as one of the best antiferroelectric thin films for energy storage applications which have been reported [2]. However, the η value in the epitaxial thin film is reduced to about 84% under the higher applied electric field (2200–2500 kV/cm) due to the slightly opened *P-E* loops. At the critical BDS value (2500 kV/cm), the epitaxial thin film has a great U_{reco} of 40.2 J/cm^3 (η = 83.8%).

Long-term reliability is also an important factor for the application of energy storage capacitors, therefore the dependence of the ferroelectric properties on the number of working cycles of the thin films has been investigated. Here, bipolar electric field cycling was used which generally causes the most severe degradation in the ferroelectric properties. The fatigue testing was performed by applying a bipolar electric field of 100 kV/cm and 100 kHz frequency. Fig. 9(a) shows that the values of net polarization ($P_{max} - P_{r+}$) of the thin films, calculated from the *P-E* loops measured at an applied electric field of 1000 kV/cm and 1 kHz, remain unchanged up to 10^{10} cycles for the epitaxial and textured PLZT thin films. Moreover, the surprising result is that the fatigue-free behavior is also observed in the polycrystalline PLZT thin film. This is different to the PLZT films grown on Pt/Si in previous studies, which the net polarization was decrease with the number of switching cycles. Several fatigue mechanisms in the fatigue behaviour

in the PLZT films have been proposed, such as the suppression of domain switching and the accumulation of oxygen vacancies upon cycling. Both mechanisms occur near the film/electrode interfaces. The suppression of domain switching is related to the pinning of the domain wall in the ferroelectric films [31,32] or the inhibition of the near-interfacial nucleation of the opposite domain switching by trapped charge [33–36]. In this study, the epitaxial and textured PLZT thin films are sandwiched between SRO electrodes and hinder the formation of the dead interfacial layer at the electrodes due to the accumulation of oxygen vacancies during the switching. In the case of PLZT thin films in this study, however, the behavior even appears to be fatigue-free for the polycrystalline thin film. This indicates that La doping can great improve the fatigue behavior of ferroelectric PLZT thin films. In the PLZT thin film, the La^{3+} dopant will occupy a lead (Pb^{2+}) site in the lattice and compensate for the oxygen vacancy (V_O) that not only inhibits the domain movement (and then reduce the remanent polarization) and also prevents the reduction in the net polarization. Accordingly, both U_{reco} and η values are also remained in the whole measurement ranges, as shown in Fig. 9(b)–(c), which indicated good fatigue behavior of the relaxor ferroelectric PLZT thin films.

As we all know, moreover, the thermal stability is also essential for the real application of dielectric capacitors. Fig. 10(a)–(c) presents the temperature dependence of ferroelectric and energy-storage properties of PLZT thin films, which was tested in the range of room temperature (~24 °C) to 200 °C. In order to avoid the capacitor break-down at elevated temperature, the measurements were performed at a low operating electric field of 500 kV/cm. As the measured temperature increasing, the slightly decrease in both U_{reco} and η values, due to the small variation in the net polarization ($P_{max} - P_{r+}$) values, are observed. The results indicate that the U_{reco} values decrease about 8.2% and 10% in the epitaxial and textured thin films and 14.2% in the polycrystalline thin film, as the temperature increases from room temperature to 160 °C. Meanwhile, the η values reduce 4.2%, 9.6% and 12.4% in the epitaxial, textured, and polycrystalline thin films, respectively. The sharp decrease of U_{reco} and η values above 160 °C may be attributed to the reduction in the polarization and the increase in the leakage current, as reflected by the rounded ends of the *P-E* loops measured at 200 °C, as shown in Fig. 10(d)–(f).

4. Conclusions

In summary, the relaxor ferroelectric PLZT thin films were fabricated using pulsed laser deposition. The study shows that the buffer and electrode layers have pronounced effect on the growth mechanism, microstructure and energy-storage performance in the PLZT thin films. The large U_{reco} of 23.2 and 21.9 J/cm^3 and high η of 91.6 and 87.8% under an applied electric field of 1500 kV/cm, respectively, for the epitaxial (on STO/Si) and textured (CNO/Si) thin films, due to high thin-film quality, dense microstructure and the coexistence of relaxor FE-AFE phase. The excellent fatigue-free properties (10^{10} cycles), high thermal stability and high break-down strengths are also observed in these devices. Even the devices based on textured film has the U_{reco} and η values slightly lower than those with epitaxial film, however, the results indicate that the textured film is also suitable for modern energy-storage technology, especially in the industrial applications due to the large-scale and low-cost production.

Acknowledgements

The authors thank Mr. Phu Le and Prof. Johan E. ten Elshof for the nanosheet deposition and Mr. Mark Smithers for performing the HRSEM experiment.

References

[1] X. Hao, J. Zhai, L.B. Kong, Z. Xu, A comprehensive review on the progress of lead zirconate-based antiferroelectric materials, Prog. Mater. Sci. 63 (2014) 1–57.
[2] C.W. Ahn, G. Amarsanaa, S.S. Won, S.A. Chae, D.S. Lee, I.W. Kim, Antiferroelectric thin-film capacitors with high energy-storage densities low energy losses, and fast discharge times, ACS Appl. Mater. Interfaces 7 (2015) 26381–26386.
[3] B. Chu, X. Zhou, K. Ren, B. Neese, M. Lin, W. Wang, F. Bauer, Q.M. Zhang, A dielectric polymer with high electric energy density and fast discharge speed, Science 313 (2006) 334–336.
[4] Y. Zhang, W. Li, W. Cao, Y. Feng, Y. Qiao, T. Zhang, W. Fei, Mn doping to enhance energy storage performance of lead-free 0.7NBT-0.3ST thin films with weak oxygen vacancies, Appl. Phys. Lett. 110 (2017) 243901.
[5] H. Zhu, M. Liu, Y. Zhang, Z. Yu, J. Ouyang, W. Pan, Increasing energy storage capabilities of space-charge dominated ferroelectric thin films using interlayer coupling, Acta Mater. 122 (2017) 252–258.
[6] N.H. Fletcher, A.D. Hilton, B.W. Ricketts, Optimization of energy storage density in ceramic capacitors, J. Phys. D: Appl. Phys. 29 (1996) 253–258.
[7] C. Liu, S.X. Lin, M.H. Qin, X.B. Lu, X.S. Gao, M. Zeng, Q.L. Li, J.-M. Liu, Energy storage and polarization switching kinetics of (001)-oriented $Pb_{0.97}La_{0.02}(Zr_{0.95}Ti_{0.05})O_3$ antiferroelectric thick films, Appl. Phys. Lett. 108 (2016) 112903.
[8] Z. Liu, X. Chen, W. Peng, C. Xu, X. Dong, F. Cao, G. Wang, Temperature-dependent stability of energy storage properties of $Pb_{0.97}La_{0.02}(Zr_{0.58}Sn_{0.335}Ti_{0.085})O_3$ antiferroelectric ceramics for pulse power capacitors, Appl. Phys. Lett. 106 (2015) 262901.
[9] Z. Hu, B. Ma, R.E. Koritala, U. Balachandran, Temperature-dependent energy storage properties of antiferroelectric $Pb_{0.96}La_{0.04}Zr_{0.98}Ti_{0.02}O_3$ thin films, Appl. Phys. Lett. 104 (2014) 263902.
[10] X. Wang, L. Zhang, X. Hao, S. An, B. Song, Dielectric properties and energy-storage performances of $(1-x)Pb(Mg_{1/3}Nb_{2/3})O_3-xPbTiO_3$ relaxor ferroelectric thin films, J. Mater. Sci.: Mater. Electron. 26 (2015) 9583–9590.
[11] Y. Liu, X. Hao, S. An, Significant enhancement of energy-storage performance of $(Pb_{0.91}La_{0.09})(Zr_{0.65}Ti_{0.35})O_3$ relaxor ferroelectric thin films by Mn doping, J. Appl. Phys. 114 (2013) 174102.
[12] L. Zhang, X. Hao, J. Yang, S. An, B. Song, Large enhancement of energy-storage properties of compositional graded $(Pb_{1-x}La_x)(Zr_{0.65}Ti_{0.35})O_3$ relaxor ferroelectric thick films, Appl. Phys. Lett. 103 (2013) 113902.
[13] X. Hao, Y. Wang, J. Yang, S. An, J. Xu, High energy-storage performance in $Pb_{0.91}La_{0.09}(Ti_{0.65}Zr_{0.35})O_3$ relaxor ferroelectric thin films, J. Appl. Phys. 112 (2012) 114111.
[14] S. Tong, B. Ma, M. Narayanan, S. Liu, R. Koritala, U. Balachandran, D. Shi, Lead lanthanum zirconate titanate ceramic thin films for energy storage, ACS Appl. Mater. Interfaces 5 (2013) 1474–1480.
[15] M.D. Nguyen, E.P. Houwman, M. Dekkers, C.T.Q. Nguyen, H.N. Vu, G. Rijnders, Enhanced energy storage density and energy efficiency of epitaxial $Pb_{0.9}La_{0.1}(Zr_{0.52}Ti_{0.48})O_3$ relaxor-ferroelectric thin-films deposited on silicon by pulsed laser deposition, APL Mater. 4 (2016) 080701.
[16] C.T.Q. Nguyen, M.D. Nguyen, H.T. Vu, E.P. Houwman, H.N. Vu, G. Rijnders, High energy storage responses in all-oxide epitaxial relaxor ferroelectric thin films with the coexistence of relaxor and antiferroelectric-like behaviors, Thin Solid Films 636 (2017) 188–192.
[17] M.D. Nguyen, H. Yuan, E.P. Houwman, M. Dekkers, G. Koster, J.E. ten Elshof, G. Rijnders, Highly oriented growth of piezoelectric thin films on silicon using two-dimensional nanosheets as growth template layer, ACS Appl. Mater. Interfaces 8 (2016) 31120–31127.
[18] C. Marchiori, M. Sousa, A. Guiller, H. Siegwart, J.-P. Locquet, J. Fompeyrine, G.J. Norga, J.W. Seo, Thermal stability of the $SrTiO_3$ & z.urule;(Ba,Sr)O stacks epitaxially grown on Si, Appl. Phys. Lett. 88 (2006) 072913.
[19] T. Shibata, H. Takano, Y. Ebina, D.S. Kim, T.C. Ozawa, K. Akatsuka, T. Ohnishi, K. Takada, T. Kogure, T. Sasaki, Versatile van der Waals epitaxy-like growth of crystal films using two-dimensional nanosheets as a seed layer: orientation tuning of $SrTiO_3$ films along three important axes on glass substrates, J. Mater. Chem. C 2 (2014) 441–449.
[20] H. Yuan, M. Nguyen, T. Hammer, G. Koster, G. Rijnders, J.E. ten Elshof, Synthesis of $KCa_2Nb_3O_{10}$ crystals with varying grain sizes and their nanosheet monolayer films as seed layers for PiezoMEMS applications, ACS Appl. Mater. Interfaces 7 (2015) 27473–27478.
[21] M.D. Nguyen, E.P. Houwman, M. Dekkers, G. Rijnders, Strongly enhanced piezoelectric response in lead zirconate titanate films with vertically aligned columnar grains, ACS Appl. Mater. Interfaces 9 (2017) 9849–9861.
[22] M.D. Nguyen, E. Houwman, M. Dekkers, H.N. Vu, G. Rijnders, A fast room-temperature poling process of piezoelectric $Pb(Zr_{0.45}Ti_{0.55})O_3$ thin films, Sci. Adv. Mater. 6 (2014) 243–251.
[23] H. Funakubo, M. Dekkers, A. Sambri, S. Gariglio, I. Shklyarevskiy, G. Rijnders, Epitaxial PZT films for MEMS printing applications, MRS Bull. 37 (2012) 1030–1038.
[24] L. Pintilie, Charge transport in ferroelectric thin films, in: M. Lallart (Ed.), Ferroelectrics – Physical Effects, InTech, Rijeka, 2011, pp. 101–134.
[25] J.F. Scott, Ferroelectric Memories, Springer, Berlin, 2000.
[26] S.M. Sze, Physics of Semiconductor Devices, John Wiley & Sons, New York, 1981.
[27] C.-K. Huang, C.-H. Chang, T.-B. Wu, On the suppression of hydrogen degradation in $PbZr_{0.4}Ti_{0.6}O_3$ ferroelectric capacitors with PtO_x top electrode, J. Appl. Phys. (2005) 104105.
[28] A. Shafiei, C. Oprea, A. Alfantazi, T. Troczynski, In situ monitoring of the effects of hydrogen on $Pb(Zr,Ti)O_3$ structure, J. Appl. Phys. 109 (2011) 114108.
[29] A. Shafiei, A. Alfantazi, Experimental investigation of the effects of water electrolysis parameters on the amount of hydrogen damage in $Pb(Zr,Ti)O_3$, J. Mater. Sci. 49 (2014) 519–526.

[30] Y. González-Abreu, A. Peláiz-Barranco, J.D.S. Guerra, P. Saint-Grégoire, Piezoelectric behavior in $Sr_{1-x}Ba_xBi_2Nb_2O_9$ aurivillius-type structure ferroelectric ceramics, Phys. Status Solidi B 250 (2013) 1551–1555.
[31] W.L. Warren, D. Dimos, B.A. Tuttle, R.D. Nasby, G.E. Pike, Electronic domain pinning in $Pb(Zr,Ti)O_3$ thin films and its role in fatigue, Appl. Phys. Lett. 65 (1994) 1018–1020.
[32] A. Gruverman, B.J. Rodriguez, R.J. Nemanich, A.I. Kingon, Nanoscale observation of photoinduced domain pinning and investigation of imprint behavior in ferroelectric thin films, J. Appl. Phys. 92 (2002) 2734–2739.
[33] A.K. Tagantsev, Cz. Pawlaczyk, K. Brooks, N. Setter, Built-in electric field assisted nucleation and coercive fields in ferroelectric thin films, Integr. Ferroelectr. 4 (1994) 1–12.
[34] A.K. Tagantsev, I. Stolichnov, N. Setter, J.S. Cross, M. Tsukada, Non-Kolmogorov-Avrami switching kinetics in ferroelectric thin films, Phys. Rev. B 66 (2002) 214109.
[35] D. Matthew, J.F. Scott, A model for fatigue in ferroelectric perovskite thin films, Appl. Phys. Lett. 76 (2000) 1060–1062.
[36] J.F. Scott, D. Matthew, Oxygen-vacancy ordering as a fatigue mechanism in perovskite ferroelectrics, Appl. Phys. Lett. 76 (2000) 3801–3803.